Share Your Innovations through JACS Directory

Journal of Nanoscience and Technology

Visit Journal at http://www.jacsdirectory.com/jnst

ISSN: 2455-0191

Removal of Cationic Dyes from Aqueous Solution by Adsorption on Mesoporous TiO_2-SiO_2 Nanocomposite

R. Ranjith, P. Shameela Rajam*

PG & Research Department of Chemistry, Bishop Heber College, Tiruchirappalli – 620 017, Tamil Nadu, India.

ARTICLE DETAILS

Article history:
Received 27 October 2017
Accepted 06 November 2017
Available online 22 November 2017

Keywords:
TiO_2-SiO_2
Cationic Dyes
Methylene Blue
Crystal Violet
Thermodynamic Study

ABSTRACT

The main objective of this work is to study the isotherm and kinetic models for the adsorption of cationic dyes like methylene blue (MB) and crystal violet (CV) on mesoporous TiO_2-SiO_2 nanocomposite. The formation of nanocomposite was confirmed using X-ray diffraction, FT-IR spectral analysis, scanning electron microscopy with energy dispersive spectra, transmission electron microscope, BET surface area and UV-Vis diffused reflectance spectra (DRS). The adsorption of MB and CV was studied in batch mode experiments and it was found to be highly dependent on solution pH, contact time, dose and concentration. The cationic dyes adsorption process followed the pseudo-second-order rate model. The Langmuir adsorption isotherm with a maximum adsorption capacity of MB and CV for 333.33 and 90.91 mg/g respectively. The thermodynamic studies reveals that the adsorption of MB and CV onto TiO_2-SiO_2 surface was spontaneous, endothermic and through a process of physisorption. The results also visible that the mesoporous TiO_2-SiO_2 nanocomposite was much more effective for the adsorption of cationic dyes, and it retained its original adsorption capacity for six successive cycles of adsorption−desorption.

1. Introduction

Water pollution is one of the most important issues in the field of environmental science due to extreme use of synthetic dues. The presence of these dyes even in low quantities cause serious health problems to flora and fauna [1]. Among various synthetic dyes pollutants, cationic dyes are the most common pollutants. These dyes are released from textile, paper, plastic, leather, and food industries [2]. MB and CV are the MB widely used cationic dyes in textile industries dyes are is toxic, carcinogenic that can cause irritation, allergy and cancer in humans. Further, CV can produce human bladder cancer and cancer in the digestive system of other animals [3]. Therefore it is need to remove those dye contaminants from effluent water. Currently, several methods are available to purify the dye polluted water such as adsorption [4], coagulation [5], flocculation [6], reverse osmosis [7], chemical oxidation [8], ozonation [9], membrane filtration [10], ion exchange [11] and electrochemical techniques [12]. Among these methods adsorption is one of the promising technique for the removal of from wastewater [13].

The semiconductor materials like TiO_2, ZnO, Fe_2O_3 and Al_2O_3 has been widely used materials in these technique owing to its unique properties especially TiO_2 has been widely studied material due to its unique properties like thermal, chemical stability, nontoxic, low cost, bandgap energy, almost similar with ZnO and also as a potential adsorption of cationic dyes [14]. The adsorption process has also some limitations like low efficiency to adsorb dyes in the waste water as a single phase semiconductor oxide. These various effects have been taken to overcome these drawbacks with doping metals, non-metals, conducting polymers to enhance the adsorption efficiency of TiO_2 [15]. Recently SiO_2 has been used various applications like optoelectronic and photocatalytic materials and also in adsorption of cationic dyes. This is due to its high thermal conductivity and large surface area. Moreover SiO_2 has recombination of TiO_2 is to increase the surface area. The combined TiO_2-SiO_2 nanocomposite shows good adsorption activity towards removal of dyes [16].

Many synthetic methods like electrostatic spray deposition, co-precipitation, hydrothermal, chemical vapour deposition, sonochemical technique, sol-gel and microwave assisted techniques have been reported for the synthesis of TiO_2-SiO_2 nanocomposites. Among these, sol-gel method could be considered as one of the most promising method, because it is easy to process, relatively low reaction temperature, energy saving, environmentally friendly and uniform particle size as compared with the other methods [17, 18].

The present work deals with the development of mesoporous TiO_2-SiO_2 nanocomposite for water clean-up process. The as-synthesised nanocomposite were characterized by, X-ray diffraction (XRD), FT-IR, scanning electron microscopy with energy dispersive spectra (SEM-EDS), transmission electron microscope (TEM), BET surface area and UV-Vis diffused reflectance spectra (DRS). The adsorption studies were assumed to find out the adsorption efficiency of the nanocomposite. The factors influencing the adsorption capacity of the composite such as pH, contact time, dose and concentrations of the cationic dyes methylene blue (MB), crystal violet (CV) were investigated. In order to examine the controlling mechanism of the adsorption process, the kinetics, adsorption isotherms and thermodynamics parameters were evaluated. Moreover, the regenerate capacity and adsorption mechanism was investigated to provide a confidence that the composites have bright prospects in dye wastewater treatment.

2. Experimental Methods

Table 1 Details of the cationic dyes of Methylene Blue (MB) and Crystal Violet (CV)

Dyes	Chemical Structure	Molecular Formula	Molecular Weight (g mol^{-1})	λ_{max} (nm)
MB	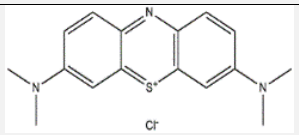	$C_{16}H_{18}ClN_3S$	19.85	663
CV	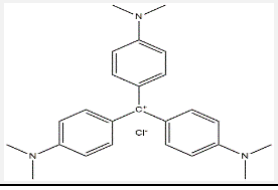	$C_{25}H_{30}N_3Cl$	407.979	586

*Corresponding Author
Email Address: shameelarajam@gmail.com(P. Shameela Rajam)

All chemicals were purchased from Sigma Aldrich Co., Ltd, analytical grade purity. Ethanol was purchased by High media chemicals, India. All solutions were prepared using double deionized water. Table 1 shows the significance details of the cationic dyes of methylene blue and crystal violet and structures of the dyes methylene blue & crystal violet.

TiO_2 synthesised by hydrothermal method, $TiCl_3$ was precursor added to DD water and drop wise added to NaOH, Purple coloured precipitate formed and stirred at 1 h, the precipitate several time washed with DD water and calcinated with 410 °C the purple precipitate changed to colourless powder formed. Mesoporous TiO_2-SiO_2 nanocomposite was prepared by the facile sol–gel method. Titanium trichloride ($TiCl_3$) and Tetraethyl orthosilicate (TEOS) were used as a precursor for TiO_2 and SiO_2, (Fig. 1). $TiCl_3$ was added to drop wise distilled water under vigorous stirring and ethanol added to TEOS these mixtures added $TiCl_3$ water solution and then added to drop wise NaOH solution, purple colour gel formed. The resulting purple gel was then taken in an alumina crucible and subjected to microwave irradiation for 30 min at a maximum power of 1000 W in a microwave accelerated reaction system. The microwave synthesis instrument IFB (Model: 25PG1S), microwave to heat the gel continuously. The system can be operated with the maximum power and frequency of 2450 MHz, respectively. The gel was changed to colourless powder. The resultant powder was heated to 110 °C in hot air oven and washed several times with distilled water and then dried at room temperature. At last, the nanocomposite white powder was calcined at 410 °C for 2 h.

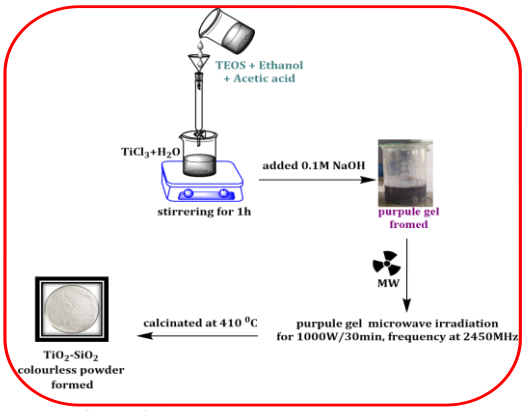

Fig. 1 Step wise synthesis of mesoporous TiO_2-SiO_2 nanocomposite

2.1 Characterization

The prepared mesoporous TiO_2-SiO_2 nanocomposite was characterized and analysed using X-ray diffraction (XRD) pattern of the powder was recorded at room temperature by a Bruker D8 X-ray diffractometer with CuKα radiation (λ = 0.15418 nm) operating at 40 kV accelerating voltage and 40 mA filament current. FT-IR spectra were recorded by using Perkin-Elmer spectrometer in the frequency range of 4000-400 cm^{-1}. The SEM-EDS structure and morphology of the obtained samples were examined by the Quanta 200 FEG High Resolution Scanning Electron Microscope (HR-SEM) with a versatile high resolution scanning electron was performed at accelerating voltage of 20 kV and an energy-dispersive X-ray spectroscopy (EDS) facility attached to the HR-SEM was employed to analyse chemical composition, High Resolution Transmission Electron Microscopy (HR-TEM); JEOL-JEM 2100 with an acceleration voltage of 120 kV, BET surface area isotherm at 77 K was investigated using a Micromeritics ASAP 2020 Porosimeter. Complete adsorption and desorption analysis. The UV–Vis diffuse reflectance spectra were obtained using JASCO UV–Vis diffused reflectance spectra (DRS) and the absorption spectra for dye adsorption were recorded by using Perkin-Elmer Lambda 35 spectrophotometer.

2.2 Batch Adsorption Studies

Batch experiments were used to examine the effects of such as effect of the pH, contact time, dose and dye concentrations. The sorption equilibrium experiments include the determination of isotherms, kinetics and thermodynamics of adsorption. In each experiment, 0.1 g of adsorbent was stirred with 50 mL of each dye solutions 50 mg/L for 60 min at 120 rpm at 303 K. The effect of pH values on the adsorption property was conducted by varying the initial pH of the solutions from 2 to 11, using 0.1 M NaOH and 0.1 M HCl. To obtain equilibrium adsorption time, samples were taken out at different time intervals (from 0 to 60 min). The effect of dose varying 0.01 g to 0.15 g. The corresponding concentration were obtained, and the adsorption kinetics curves were also plotted. After the equilibrium, the two phases were separated and the concentration of dyes were analysed by using spectrophotometer. The samples were analysed in replicates of three. The following equations were used for calculating the removal percentage of dyes and the adsorption capacities. MB and CV were used to evaluate the adsorption capacity of the obtained materials TiO_2-SiO_2 composite. For each adsorption study, a 10 mL of 50 mg/L the dyes aqueous solution were mixed with a certain weight of adsorbent. The dyes concentration was analysed using UV–Visible spectrophotometer at the λ_{max} = 664 nm for MB and 587 nm for CV. The adsorption efficiency (q_e) of MB and CV on mesoporous TiO_2-SiO_2 composite was calculated from the following equations:

$$q_e = \frac{(C_0 - C_e)V}{m} \quad (1)$$

$$\text{Re}moval\ \% = \frac{(C_0 - C_e)}{C_0} \times 100\ \% \quad (2)$$

where m (g) is the weight of adsorbent applied, V (L) is the solution volume and q_e (mg/g) is the adsorption amount at equilibrium state. C_o and C_e (mg/L) are the concentration of dyes at initial and equilibrium states, respectively.

The adsorption isotherm indicates the adsorbing molecules distribute between the liquid phase and the solid phase when the adsorption process range an equilibrium state. Adsorption isotherm were carried out as batch test by adding an optimum amount (0.05 g) of adsorbent to a series of 50 mL brown bottle filled with 10-50 mg/L of dye solutions at 308 K. Langmuir, Freundlich and D-R isotherm models were analysed to the adsorption equilibrium.

3. Results and Discussion

3.1 XRD Analysis

X-ray diffraction of Fig. 2(a) shows that the TiO_2 nanoparticles had the anatase crystalline structure, while there was no classifiable peak that could be attributed to formation of other crystalline structures of TiO_2. TiO_2 diffraction peaks appear at (2θ) 25.32, 36.92, 37.76, 48.06, 53.86, 55.06, 62.64, 68.78, 70.44, and 75.06, its planes corresponding to (101), (103), (004), (200), (105), (211), (204), (116), (220) and (215) these planes clearly denoted anatase phase of TiO_2 and matched to JCPDS No. (21-1272) [19] and its size was calculated around 14-20 nm. XRD image of the mesoporous TiO_2-SiO_2 less than 15 % of TiO_2 dioxide in the structure show a broad signal 23^0 (2θ) due to amorphous silica (Fig. 2(b)) [20].

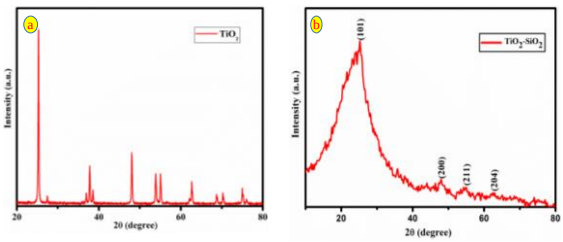

Fig. 2 XRD of the (a) TiO_2 and (b) mesoporous TiO_2-SiO_2 nanocomposite calcinated with 410 °C for 2 h

Furthermore, TiO_2 overlap of overwhelmed peak related to SiO_2 in the XRD pattern indicated that SiO_2 in the identified was structurally amorphous. At lower percentage of TiO_2 broad peak gradually appear at 2θ = 25^0, 48^0, 54^0 and 62^0 corresponding to the (101), (200), (211) and (204) crystal planes reflection of anatase no reflection of rutile was detected. [21, 22], heat-treatment was identified as TiO_2 in anatase phase and amorphous silica was perfectly matched in the XRD pattern JCPDS No. 21–1272 upon calculation using the Scherrer's equation, the average size of mesoporous TiO_2-SiO_2 nanocomposite was determined to be around 10 nm.

$$D = \frac{k\lambda}{\beta\, Cos\theta} \quad (3)$$

where D is the average crystallite size (nm), where k is a constant equal to 0.89, λ is the applied X-ray wavelength (λ = 0.15406Å), θ is the diffraction angle, the full width at half maximum intensity (FWHM), and, the half diffraction angle.

3.2 FT-IR

The FT-IR spectra of the TiO_2 shown in Fig. 3(a). Ti-O-Ti vibration at 674 cm^{-1}, the absorption in the range from 3500 to 2500 cm^{-1} may be related to the presence of O-H stretching vibration (Monomer, intermolecular and intra molecular). The absorption band at 1637 cm^{-1} due to the presence of O-H bending vibration which is probably because of the reabsorption of

water from the atmosphere has occurred [23]. The Fig. 3(b) shows FT-IR spectra of mesoporous TiO_2-SiO_2 nanocomposite, the peak at 3477 cm^{-1} stretching and bending vibration is assigned to be -OH group and molecular H_2O, respectively. Ti-O-Ti bonds appeared in the range of 600-400 cm^{-1}, in the IR spectrum of TiO_2-SiO_2 composite. The peak at 1075 cm^{-1} which corresponds to Si-O asymmetric stretching vibration. The symmetrical Si-O-Si stretching vibration was appeared at 795 cm^{-1} [24]. The peak in the range of 960-910 cm^{-1} was contributed to the formation of Si-O-Ti bonds.

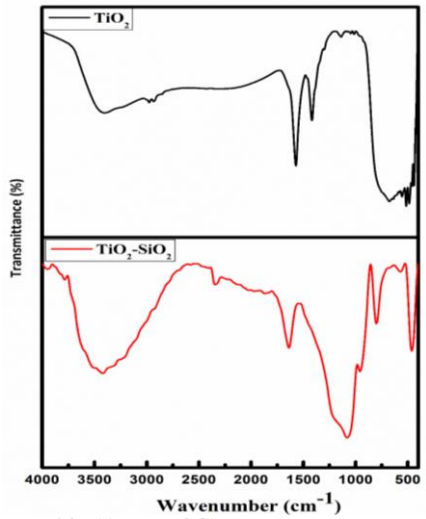

Fig. 3 FT-IR spectra of the (a) TiO_2 and (b) mesoporous TiO_2-SiO_2 nanocomposite calcinated with 410 °C for 2 h

3.3 Morphological Investigations HR-SEM and HR-TEM

Fig. 4(a-c) shows high resolution-scanning electron microscopy (HR-SEM) images of synthesised TiO_2 and mesoporous TiO_2-SiO_2 nanocomposite. Fig. 4(a) shows the SEM image of TiO_2 nanoparticles and fairly homogeneous granular porous surface with fine grain boundaries, and the mesoporous TiO_2-SiO_2 nanocomposite different size of closely packed nanoparticles and porous nature is shown in Fig. 4(b), its visibly observed the composite mesoporous nature and micro sphere like structure, [25, 26] and Fig. 4(c) show the EDS spectra and its inset image show the composition of mesoporous TiO_2-SiO_2 nanocomposite, titanium has lower molecular weight due to higher percentage of silica presence and it controlled to titanium [27, 28].

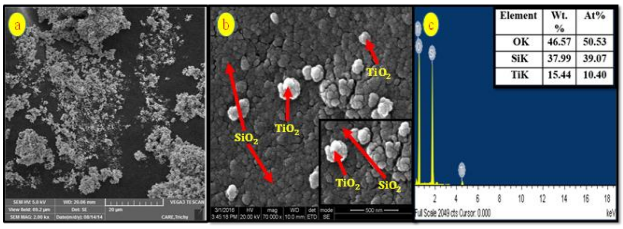

Fig. 4 HR-SEM images of (a) TiO_2 (b) mesoporous TiO_2-SiO_2 nanocomposite morphology according to the different magnifications, and (c) show EDS of mesoporous TiO_2-SiO_2 nanocomposite

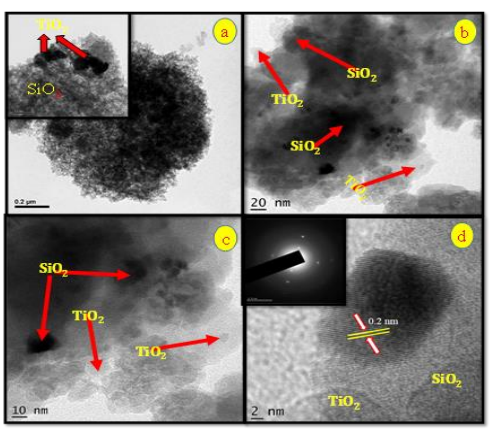

Fig. 5 HR-TEM images of (a-d) mesoporous TiO_2-SiO_2 and (d) inset image shows the corresponding SAED patterns of mesoporous TiO_2-SiO_2 composite

Fig. 5 shows HR-TEM images of TiO_2-SiO_2 composite after calcination at 410 °C for 2 h. Fig. 5(a) and its inset image show TiO_2 particles self-possessed with SiO_2 and lightly spread on the surface. These images reveals that the TiO_2-SiO_2 micro sphere consist of crystalline TiO_2 and amorphous SiO_2 nanoparticles, TiO_2 in both images clearly observed as randomly oriented and overlapping each other [29]. The TiO_2 crystals were homogenously surrounded by amorphous SiO_2 and the close connection specifies that the composites possess a highly distributed state between TiO_2 and SiO_2. Fig. 5(b) and (c) shows the particles were scattered slightly and subsequently interface of amorphous and a similar results were confirmed by SEM images, as shown in Fig. 5(a-b) [30]. Fig. 5(d) inset shows the corresponding finger print region and selected area electron diffraction (SAED) pattern. The TiO_2-SiO_2 composite indicates a better crystalline materials [31, 32].

3.4 BET Surface Area Analysis

Fig. 6(a) presents the BET Surface area of TiO_2. Based on BET analysis, the specific surface area of the fabricated TiO_2 is thus revealed to be about 9.99 m^2g^{-1}. A type-IV isotherm and H_1-type hysteresis loop were confirmed for both TiO_2 nanostructures (Fig. 3), suggesting mesoporosity in anatase TiO_2 [33]. Fig. 6(b) shows the mesoporous TiO_2-SiO_2 nanocomposite BET surface area analysis, the specific surface area is 432.34 m^2g^{-1}. The isotherm of mesoporous TiO_2-SiO_2 nanocomposite is type IV. In this type indicates the presence of mesoporous size of the hysteresis loop. It is a H_2 type with a triangular shape and a steep desorption branch [34, 35]. Such behaviour is observed for many porous inorganic oxides and has been attributed to the pore connectivity effects. Indeed, the H_2 hysteresis loops have been observed for materials with relatively uniform channel-like pores, when the desorption branch occurs in the nearby of a lower pressure limit of adsorption desorption hysteresis. The shape of the hysteresis loop for this binary oxide clearly indicates some pore blocking. Hence, it could be determined that the particles of the sample was characterized by the external surface of the narrow particles. The BET surface area, pore radius and pore volume values are summarized in Table 2 [36, 37].

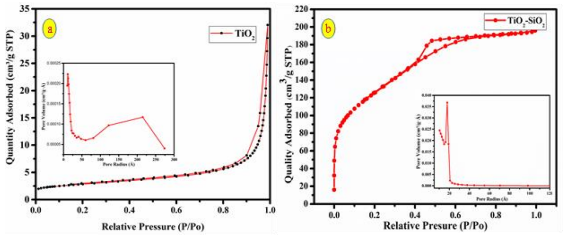

Fig. 6 BET surface area analysis of (a) TiO_2 and (b) mesoporous TiO_2-SiO_2 nanocomposite and insert of the images the BJH pore radius

Table 2 BET surface area of TiO_2 and mesoporous TiO_2-SiO_2 nanocomposite

Sample	S_{BET} (m^2 g^{-1})	R_{pore} (nm)	V_{pore} (cm^3 g^{-1})
TiO_2	9.99	11.193	0.049
TiO_2-SiO_2	432.34	1.531	0.303

S_{BET} – Specific BET surface area, R_{pore} - Pore Radius, V_{pore} – Pore Volume

3.5 Optical Properties

The optical absorbance of the nanocomposites were investigated by UV-vis diffuse reflectance spectra (DRS) Fig. 7(a). Shows the optical absorption spectra of mesoporous TiO_2-SiO_2 nanocomposite recorded in the wavelength region 375–800 nm. The visible light absorption wavelength around 288 nm, 340 nm was recorded for the TiO_2, TiO_2-SiO_2 nanocomposite respectively. The light absorption edges of hybrid TiO_2-SiO_2 show a small shift towards higher wavelength side in the visible range compared to TiO_2-SiO_2. The presumable shift in the optical absorption towards visible region after TiO_2-SiO_2 Infuse favour of adsorption [38-40]. Using the optical spectra, the band gap energy (Eg) was evaluated from the equation.

$$\alpha = A\,(h\nu - Eg)^{n}/h\nu \qquad (4)$$

Fig. 7(b) shows the plot of hν versus $(\alpha h\nu)^2$ A plot of the transformed Kubelka–Munk function as a function of energy of light was roughly estimated, the direct band gap for TiO_2 was 3.2 eV, and it slightly decreased to 3.05 eV after SiO_2 addition, proposing that, TiO_2 ions in the valance band work as defect sites to decrease the band gap. Introducing SiO_2 into TiO_2 lattice to produce additional electronic states in the oxide energy band gap cause changes in optical transitions and a red-shift in absorption spectrum. Nevertheless these results show that the strong absorption intensity of light for the mesoporous TiO_2–SiO_2 nanocomposite suggested that they could have higher adsorption activity for a given reaction.

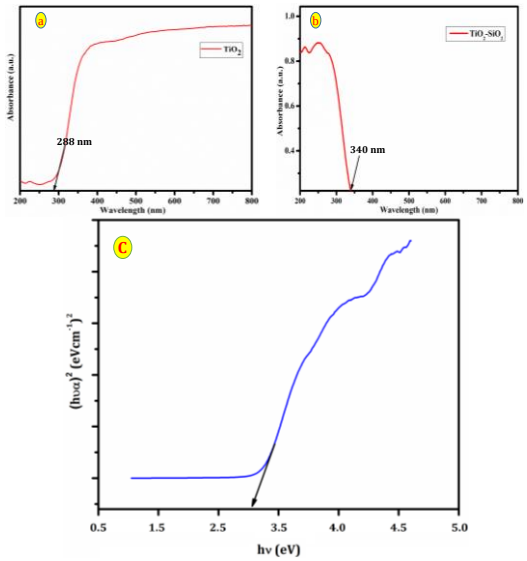

Fig. 7 UV-Vis DRS spectra of (a) TiO_2 and (b) mesoporous TiO_2-SiO_2 nanocomposite (C) Optical band gap of TiO_2-SiO_2

3.6 Adsorption Studies

3.6.1 Effect of pH

In order to investigate the effect of pH of solution on cationic dyes methylene blue and crystal violet and to determine the adsorption behaviour of the dyes, tests were carried out at predetermined experimental conditions taking initial dyes concentration as 50 mg/L. Solutions of NaOH and HCl were employed to adjust the pH of the test solutions. In the case of adsorption of dyes on mesoporous TiO_2-SiO_2 nanocomposite a pH range from 2 to 11 was selected. Dye molecules, with the increase of pH from 5 to 11, increase the adsorption accurse. Due to neutralization of the negative charge at the surface of the adsorbent by the positively charged dyes molecules. An increased diffusion process facilitates dye attachment at the active sites of the adsorbents. Fig. 8(a) clearly reveal that with further increase in pH from 8 to 11, the adsorption process attains equilibrium. Simple conditions favour adsorption of dyes, thus pH - 8 and pH - 9 were considered as optimum pH for the dye MB and CV.

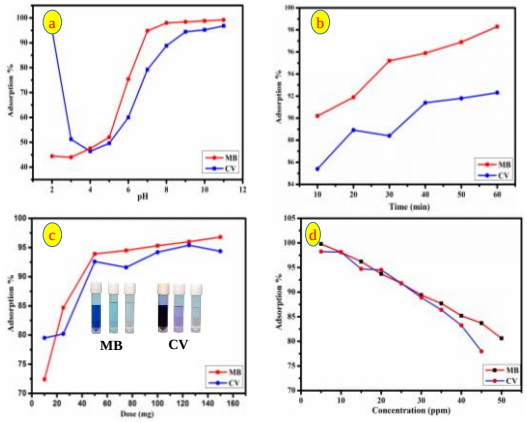

Fig. 8 Adsorption effects of (a) pH, (b) contact time, (c) dose (d) concentration for MB and CV adsorption onto mesoporous TiO_2-SiO_2 composite

3.6.2 Effect of Contact Time

The effect of contact time on the adsorption efficiency of MB and CV solutions the mesoporous TiO_2-SiO_2 nanocomposite dosage of 0.1 g, at the optimum pH and initial dye concentration of 50 mg/L by fixing at temperature 308 K. As can be seen from Fig. 8(b), the plot indicated a major part of the adsorption process appeared in the early 30 min (MB) and 40 min (CV). Furthermore, the adsorption had reached the saturated adsorption until 30 and 40 min. Hence 30 min for MB & 40 min for CV chosen to be the equilibrium time for cationic dyes.

3.6.3 Effect of Dose

The study of the effect of dose of the adsorbent was necessary in order to observe a minimum possible amount which shows maximum adsorption. The amounts of the adsorbent were varied from 0.01 to 0.15 g. In this experiment, the adsorptive ability of the adsorbents at a concentration 50 mg/L dyes solutions at optimum pH for temperature 303 K were considered. Fig. 8(c) show an increase in the amount of the adsorbents lead to an increase in the amount of the dyes adsorbed, in both dyes with 0.05 g of the adsorption 93.9 % for MB 92.6 % have been removed.

3.6.4 Effect of Concentration

Effect of concentration of both dyes were studied at different concentrations varying from 5 mg/L to 50 mg/L at fixed optimum dose, optimum pH, equilibrium time and room temperature were carried out at 308 K. Fig. 8(d) show the maximum efficiency and then it was observed at lower concentration, which decreases with the increase in substrate concentration.

3.7 Adsorption Equilibrium Study

The adsorption isotherms demonstrate the specific relation between the adsorption capacity of an adsorbent and the concentration of adsorbate at a constant temperature. The Langmuir, Freundlich and D–R isotherm models were used to study adsorption behaviour.

3.7.1 Langmuir Isotherm

Langmuir isotherm contribute more satisfactory fitting to the adsorption isotherms of the cationic dyes on mesoporous TiO_2-SiO_2 nanocomposite adsorbent with correlation coefficient (R^2) was higher than 0.99, indicating a good agreement of the data. Thus it may be concluded that Langmuir model is suitable to describe the adsorption of MB and CV on mesoporous TiO_2-SiO_2 nanocomposite, which emphasizes the formation of monolayer coverage of dyes molecules at specific homogeneous sites on the adsorbent surface. They can be described as follows.

$$\frac{C_e}{q_e} = \frac{1}{K_L q_m} + \frac{C_e}{q_m} \quad (5)$$

The Langmuir isotherm can be linearized for

$$\frac{1}{q_e} = \frac{1}{K_L q_m} + \frac{1}{q_m} \quad (6)$$

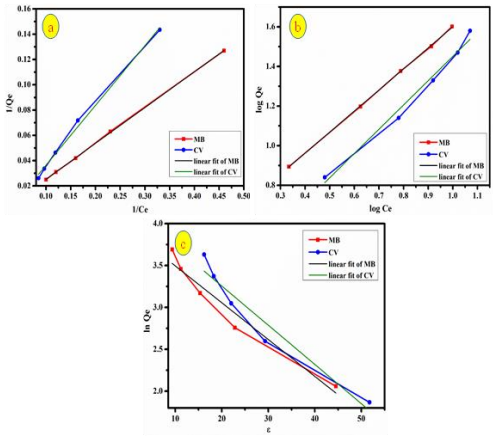

Fig. 9 Adsorption Isotherm models of (a) Langmuir, (b) Freundlich and (c) D-R for MB and CV adsorption onto mesoporous TiO_2-SiO_2 composite

where, q_e is the amount of adsorption at equilibrium (mg/g), C_e is the dye concentration at equilibrium K_L is the Langmuir adsorption constant (L/mg) and q_m is the theoretical maximum adsorption capacity (mg/g). A graph between $1/q_e$ vs. $1/C_e$ was plotted and the constants q_m and K_L were obtained from slope and the intercept (Fig. 9(a)). The value of q_m, K_L constants, R^2 are presented in Table 2. The maximum monolayer adsorption capacity q_m for TiO_2-SiO_2 composite was 333.33 (MB) and 90.91 (CV) mg/g respectively [41]. The value of q_m obtained in the present study is within the range of the values reported in the literature for the adsorption of MB and CV by various adsorbents as given in Table 3.

Table 3 Langmuir, Freundlich and D–R isotherm models for MB and CV adsorption by mesoporous TiO_2-SiO_2 nanocomposite

Dyes	Langmuir				Freundlich			D–R			
	q_m (mg/g)	K_L (L/mg)	R_L	R^2	K_F (mg/g)	1/n	R^2	q_m (mg/g)	β (mol²/kJ²)	E (kJ/mol)	R^2
MB	333.3	0.011	0.90 to 0.65	0.99	3.44	0.94	0.99	3.94	0.044	3.38	0.97
CV	90.91	0.023	0.81 to 0.46	0.99	1.68	0.82	0.98	4.06	0.021	4.9	0.93

The results revealed that the mesoporous TiO_2-SiO_2 nanocomposite had the highest adsorption ability. The reason was attributed to its small particle size and large surface area. It has been reported that the smaller particle size solid enhanced better migration and interaction of the adsorbate to the active adsorbent sites than the longer one. The essential feature of the Langmuir isotherm may be expressed in terms of a dimensionless constant called separation factor (R_L), studies on which is given by the following equation.

$$R_L = \frac{1}{1+(K_L \times C_0)} \quad (7)$$

R indicates the shape of the isotherm to be either linear (R_L =1), unfavourable (R_L >1), favourable (0 < R_L < 1), or irreversible (R_L = 0) [42]. In the present study, R_L values obtained were in the range of MB for 0.65–0.90 and CV for 0.46-0.81, indicating favourable adsorption of dye on different mesoporous TiO_2-SiO_2 nanocomposite. Comparison of adsorption capacities of different adsorbents for MB and CV at 308 K are represented in Table 4.

Table 4 Comparison of adsorption capacity of MB and CV on various adsorbents

Dyes	Adsorbents	q_m (mg/g)	Ref.
	CNT	35.00	[43]
	TiO_2 nanotube	57.14	[44]
MB	ZnO-PANI	20.55	[45]
	zeolite	28.90	[46]
	TiO_2-SiO_2	333.33	This work
	Ch–GO	64.935	[47]
	Magnetic nanocomposite	81.70	[48]
CV	organoclay	365.11	[49]
	FMWCNT	100.00	[50]
	TiO_2-SiO_2	90.91	This work

3.7.2 Freundlich Isotherm

Freundlich model is a multilayer model and provides the details of interaction between adsorbate and the active sites of the adsorbent with the broad range of adsorbate concentrations. It is also useful to investigate the surface heterogeneity of adsorbent and represented as given below [51].

$$\log q_e = \log K_F + \frac{1}{n}\log C_e \quad (8)$$

where q_e (mg/g) is the adsorption capacity, which usually refers to the quality of the solvent adsorbed per unit mass of adsorbent C_e (mg/L) is the concentration of MB and CV when the adsorption equilibrium is achieved K_F and n are Freundlich adsorption constants related to the adsorption capacity and intensity of the adsorbents respectively. A plot of log q_e vs. log C_e gives a straight line with the slope ($1/n$) and intercept (log K_F). The estimated constants K_F and n values are represented in Table 3 and fitted isotherm was shown in Fig. 9(b). The slope ($1/n$) value range of 0-1 is used to determine the surface heterogeneity and heterogeneity is high if the slope value is closer to zero [52]. The values of K_F obtained in this study were 3.44 & 1.68 and that of $1/n$ were 0.94 & 0.82 indicates that the adsorption of MB and CV by mesoporous TiO_2-SiO_2 nanocomposite was favoured by positive cooperative binding and heterogeneous nature [53].

3.7.3 D-R Isotherm

D-R isotherm is usually employed to explain the mechanism of adsorption with respect to Gaussian energy distribution onto a heterogeneous surface and to determine the nature of adsorption as physical or chemical based on the free mean sorption energy [54]. Eq.(8) is D-R isotherm model and is expressed as,

$$\ln q_e = \ln q_m - \varepsilon\beta^2 \quad (9)$$

where q_e is the equilibrium dyes concentration on the adsorbent (mol/g), q_m is the maximum adsorption capacity of the adsorbent (mol/g), β is the activity coefficient related to the mean free energy of sorption (mol²J²) and ε is Polanyi potential. The value of ε can be calculated from the following relation [55].

$$\varepsilon = RT(1+1/C_e) \quad (10)$$

where R is gas constant,(8.314/J/mol/K), T is temperature (K) and C_e is the equilibrium dyes concentration in solution (mol/L). The activity coefficient β was further used to calculate the sorption free energy E (kJ/mol) which is required to transfer the sorbate to the surface of the sorbent from infinity in the solution, and the E value can be calculated using the following equation:

$$E = \frac{1}{\sqrt{2\beta}} \quad (11)$$

Fig. 9(c) represent the D-R isotherm models of the adsorption of TiO_2-SiO_2 composite onto the metals under study. The values of q_m and E are given in Table 3. The mean free energy gives information about sorption mechanism whether it is physical or chemical. If E value lies between 8 k/mol and 16 kJ/mol, the sorption takes place chemically, and while if E is less than 8 kJ/mol the sorption process is physical in nature. Table 1 shows that the E values of all the dyes under study are less than 8 kJ/mol indicating that mechanism is physisorption [56].

All the investigated isotherms fitted well with the experimental data having regression coefficient (R^2) above 0.9. Table 3 was an evident that Freundlich isotherm (R^2 = 0.957) was the best fitted model and the maximum adsorption capacity of 333.33 and 90.91 mg/g were observed from the Langmuir isotherm for the adsorption of MB and CV by TiO_2-SiO_2 composite.

3.8 Adsorption Kinetics

The kinetics of adsorption describes the rate of adsorbate application on to the adsorbent with the equilibrium time. The kinetic parameters are useful for the prediction of adsorption rate, which gives important information for designing and modelling the processes. Adsorption kinetics studies provides an understanding of adsorption rate and controlling mechanism of the process. The adsorption kinetics of MB and CV onto the mesoporous TiO_2-SiO_2 nanocomposite was investigated by employing pseudo-first order, pseudo-second order and intra-particle diffusion models.

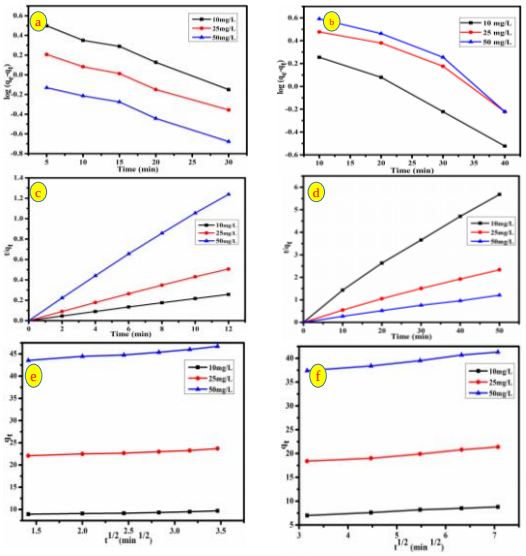

Fig. 10 (a - b) kinetic constants of pseudo-first order, (c - d) pseudo-second order and (e - f) intra-particle diffusion models for MB and CV adsorption onto mesoporous TiO_2-SiO_2 composite

3.8.1 Pseudo-First Order Model

Pseudo-first order model are represented in the following Eq.(12). The Lagergren's kinetic equations are the most common models used to describe the adsorption in liquid-solid systems, where the adsorption clearly depends on the solid capacity. Lagergren's pseudo-first order rate equation for a liquid-solid adsorption system is generally expressed as equation.

$$\log(q_e - q_t) = \log q_e - k_1 \frac{t}{2.303} \quad (12)$$

The pseudo-first order rate constant k_1 and q_e can be determined from slope and intercept of the graph by plotting log (q_e - q_t) vs. time. Pseudo-first order kinetic data was shown in Fig. 10(a) and (b) these are not found to fit pseudo-first order kinetics [57].

3.8.2 Pseudo-Second Order Model

The kinetic rate equation for pseudo-second order model predict the adsorption behaviour and is represented by the following equation (Eq. (13))

$$\frac{t}{q_t} = \frac{1}{k_2 q_e^2} + \frac{1}{q_e}t \quad (13)$$

Table 5 Kinetic constants of pseudo-first order, pseudo-second order and Intra-particle diffusion models for MB and CV adsorption by mesoporous TiO_2- SiO_2 nanocomposite

Kinetic modal	Parameters	MB			CV		
		10 mg/L	25 mg/L	50 mg/L	10 m g/L	25 mg/L	50 mg/L
First oder	q_e(exp)	9.96	23.7	46.7	8.80	21.4	41.30
	q_e(cal)	1.12	2.328	4.78	3.60	5.99	8.57
	k1	-0.15	-0.16	-0.18	0.061	0.053	0.061
	R^2	0.93	0.97	0.94	0.99	0.92	0.92
Second order	q_e(exp)	9.69	23.7	46.7	8.80	21.4	41.30
	q_e(cal)	9.83	23.98	47.39	9.452	22.42	42.92
	k2	0.318	0.16	0.08	0.025	0.015	0.012
	R^2	0.99	0.99	099	0.99	0.99	0.99
Intra-particle	q_e(exp)	9.69	23.7	46.7	8.80	21.4	41.30
	q_e(cal)	8.391	20.971	41.39	5.539	15.69	33.97
	$k_{i/d}$	0.3487	0.7425	1.4664	0.47	0.78	1.04
	R^2	0.9402	0.9667	0.9743	0.99	0.98	0.99

The pseudo-second order rate constant k_2 and q_e can be determined from intercept and slope of the graph plotted between t/q_t vs. time, Fig. 10(c) and (d) shows the adsorption kinetics is best to describe by pseudo-second order model for MB and CV adsorption by TiO_2-SiO_2 composite fitted and suggested that the adsorption of MB and CV may be due to electrostatic attraction between the charged surface and charged dyes molecules [58] .The various parameters calculated from the pseudo-first and second order models, and their regressions coefficients are given in Table 4. The regression values shows that the pseudo-second-order model to be a better fitted one than the first-order model.

3.8.3 Intra-Particle Diffusion Model

An empirical relationship, common to most adsorption processes, is that the sorbate uptake varies almost proportionally with $t^{1/2}$ and is given by Weber Morris plot *t*. The parameters obtained from intra-particle diffusion model are summarized in Table 5. The intra-particle diffusion model can be written is Eq.(14)

$$q_t = k_{id} t^{1/2} + C \qquad (14)$$

The intra-particle diffusion rate constant k_{id} (mg/g $min^{1/2}$) and boundary layer thickness constant *C* (mg/g) was obtained from the slope and intercept of the plot q_t vs. $t^{1/2}$ [59].

Fig. 10(e) and (f) reveals the regression values, it is well known understood that intra-particle diffusion does play a major role in the adsorption of various dye molecules by mesoporous TiO_2-SiO_2 nanocomposite indicate the cationic dyes molecules diffusion resistance increases and diffusion rate decreases, and adsorption equilibrium is reached finally.

3.9 Thermodynamics Study

The thermodynamics of the adsorption of MB and CV onto mesoporous TiO_2-SiO_2 nanocomposite was studied with adsorbent dose of 0.05 g, initial dyes concentration 10 - 50 mg/L, pH - 8.0 and pH - 9.0 for MB, CV respectively; predetermined shaking time and in temperature range 298, 308 and 318 K. Effect of temperature on the adsorption capacity of MB and CV were shown in Fig. 11. In general the thermodynamic parameters, namely standard Gibbs free energy change (ΔG°), enthalpy change (ΔH°) and entropy change (ΔS°) of adsorption process are calculated by using the following equations [60].

$$\ln K_D = \frac{qe}{Ce} \qquad (15)$$

$$\Delta G^0 = -RT \ln K_D \qquad (16)$$

$$\ln K_D = \frac{\Delta S^0}{R} - \frac{\Delta H^0}{RT} \qquad (17)$$

where K_D is the distribution coefficient (g/L), q_e is the adsorption capacity at equilibrium, C_e is the concentration of the dye solution at equilibrium, *T* is the temperature (K), and *R* is the gas constant respectively. However, calculation of thermodynamic parameters using K_D with dimension is controversial, if the adsorption takes place from aqueous solution. The Gibbs free energy ($\Delta G°$) for the adsorption process was calculated using Eq.(16). The Van't Hoff plot ln K_D vs. $1/T$ is used for determination of ΔH^0 and ΔS^0 values from the slope and intercept also using Eq.(17). The calculated values of thermodynamic parameters of the dyes-TiO_2-SiO_2 composite system are given in Table 6. The negative ΔG^0 values at different temperatures indicate that the adsorption process is spontaneous. The ΔG^0 values are found to be in the range of -1.5 to -3.4 kJ/mol. These values indicates that adsorption of the dyes on TiO_2-SiO_2 composite system is physisorption. The ΔG^0 value becomes more negative with increase in temperature indicating increase in percentage of adsorption with increase in temperature. The ΔH^0 value was found to be 21.7835 kJ/mol (MB) and 8.8852 kJ/mol (CV) which also supports that the adsorption process is governed by physisorption as the ΔH^0 value in the range of 1 - 93 kJ/mol indicates physisorption. The positive value of ΔH^0 specifies that the process is endothermic [61]. The positive value of ΔS^0 is attributed to the increased randomness. All the thermodynamic parameters mentioned above show that mesoporous TiO_2-SiO_2 nanocomposite could be used as a high-efficiency adsorbent to eliminate MB and CV from aqueous solution.

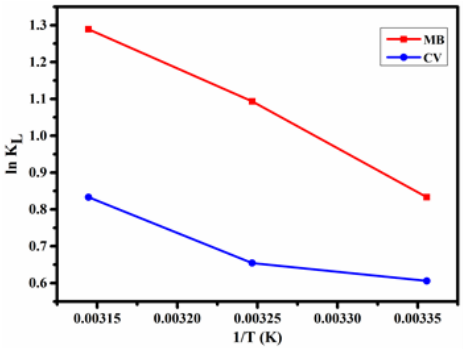

Fig. 11 Van't Hoff plots for adsorption of MB and CV onto mesoporous TiO_2-SiO_2 composite

Table 6 MB and CV Thermodynamic parameters of ΔG^0, ΔH^0 and ΔS^0 of mesoporous TiO_2-SiO_2 nanocomposite

Dyes	Temperature (K)	ΔG^0 (kJ/mol)	ΔH^0 (kJ/mol)	ΔS^0 (kJ/mol/K)
	298	-2.0638		
MB	308	-2.8000	21.7835	67.355
	318	-3.4085		
	298	-1.5012		
CV	308	-1.6757	8.8852	34.6694
	318	-2.2023		

3.10 Desorption and Regeneration Experiments

Fig. 12 shows that a practical point, repeated availability of an adsorbent is crucial to its application. According to the results obtained from the study of effect of surface potential and pH, the composites are highly pH dependent. The desorption capacity for cationic dyes from the composite is rather low, and the MB and CV adsorbed could be free in low pH solution, while the good desorption capacity from the composite can be obtained in high pH solution, thus obtaining the possibility of regeneration of the composites. In present work, 1 mol/L HCl is taken as the eluting agent and 1 mol/L NaOH as the activator were applied to investigate the adsorption stabilities of the mesoporous TiO_2-SiO_2 nanocomposite. The results are triplicated. Fig. 12 shows that the composite could be used for six cycles without significant adsorption capacity loss, concluding that the regeneration method by HCl-elution and NaOH-activation is available, and the composite prepared own excellent stability and outstanding recycle possibility [62].

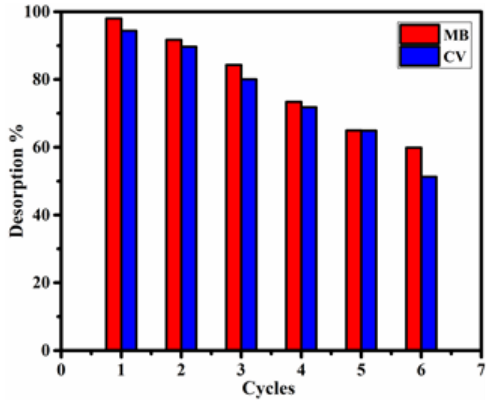

Fig. 12 Desorption cycles of MB and CV on to mesoporous TiO_2-SiO_2 composite

3.11 Adsorption Mechanism

The adsorption mechanism is greatly related to the structure and properties of the adsorbate and the adsorption of cationic dyes results from the formation of an ion pair between the cations and functional

groups presented in the adsorbent. Fig. 13(a) shows the FTIR spectra of mesoporous TiO_2-SiO_2 nanocomposite before and after methylene blue and crustal violet adsorption. No significant change was observed in intensity and wavenumber in the peak related to O-Ti-O bonding by the adsorbed molecules. The interface of the molecules of methylene blue, crystal violet and the mesoporous TiO_2-SiO_2 nanocomposite surface can occur between the free-electron pair of the oxygen of the surface group and the delocalized π-π stacking interaction between the methylene blue and crustal violet molecules and the aromatic rings of the carbon structure. Electrostatic interaction forces between dye molecules and the adsorbent structure may be involved because the dyes molecules have a positive net charge and the adsorbent has a negatively charged surface [63]. The FT-IR spectra of the MB, CV and mesoporous TiO_2-SiO_2 nanocomposite before and after adsorption are shown in Fig. 13(a). The broad band around 3462 cm^{-1} and the narrow band around 1640 cm^{-1} may be assigned to the A-OH stretching vibration and bending vibrations of adsorbed water involved in the formation of hydrogen bonding. A broad peak located at 1085 cm^{-1} which is attributed to asymmetric Si-O-Si vibrations. As an active group, Si-O-Si group could bring a relatively small but permanent negative charge, which will facilitate the electrostatic interaction between the cation dye and the negative surface of TiO_2-SiO_2. After adsorption of MB and CV.

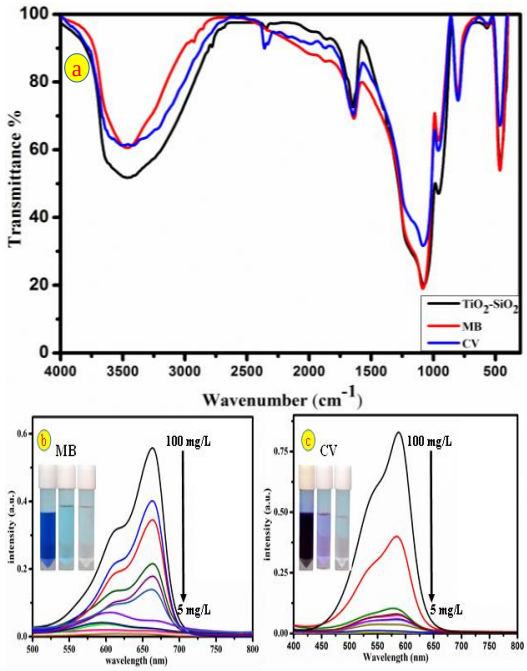

Fig. 13 After adsorption of (a) FT-IR spectra and (b-c) UV-Vis absorption spectra of MB & CV

According to the structure and properties of the adsorbate and adsorbent, the possible adsorption mechanism of CV on TiO_2-SiO_2 can be illustrated as follow: (1) electrostatic interaction between the presence of positive charge ($-N^+$) on cationic dye and the negative charge on TiO_2-SiO_2 presented by ion exchange or Si–O–Si structures. (2) Hydrogen bonding between the nitrogen atom on dyes and A-OH on the surface of mesoporous TiO_2-SiO_2 nanocomposite [64]. Fig. 13(b-c) shows temporal changes of UV–Vis absorption spectra during adsorption process of MB and CV. It revealed that the bands at 664 nm for MB and 587 nm was CV decreased markedly and almost disappeared completely after 30 min for MB & 40 min for CV adsorption process of mesoporous TiO_2-SiO_2 nanocomposite which confirms the adsorption pathway via aromatic ring opening of MB and CV dyes [65].

4. Conclusion

In this summary, mesoporous TiO_2-SiO_2 nanocomposite was successfully synthesized via a facile sol-gel method and were characterized. The adsorption data of MB and CV were well described by the pseudo-second-order kinetic model, indicating the chemical adsorption mechanism. From the adsorption data, the highest adsorption capacity of this composite is 333.33 and 90.91 mg/g that is significantly one of the better reported adsorbents for MB and CV removal. Thermodynamic parameters illustrated the entire adsorption process were endothermic and spontaneous. The mesoporous TiO_2-SiO_2 nanocomposite material was an economical and eco-friendly material. The adsorption-desorption process was repeated thrice, the composites still had a high adsorption capacity. The mesoporous TiO_2-SiO_2 nanocomposite material has been proved to be a promising material for the wastewater treatment exhibit high adsorption activity of the cationic dyes of MB and CV dyes from aqueous solutions.

Acknowledgement

This work was financially supported to Fellowship RGNF – UGC India. The authors thank the Principal, Management and PG & Research Department of Chemistry, Bishop Heber College, for the facilities provided to carry out this work, Thanks to SAIF- IIT-Madras for SEM-EDS and TEM instrumentation.

References

[1] X. Zhang, Y. Zhang, L. Zhou, X. Li, X. Guo, In situ C, N-codoped mesoporous TiO_2 nanocrystallites with high surface areas and worm-like structure for efficient photocatalysis, J. Porous Mater. (2017) 1-9.
[2] U. Pal, A. Sandoval, S. I. U. Madrid, G. Corro, V. Sharma, P. Mohanty, Mixed titanium, silicon, and aluminium oxide nanostructures as novel adsorbent for removal of rhodamine 6G and methylene blue as cationic dyes from aqueous solution, Chemosphere. 163 (2016) 142-152.
[3] T. Yao, S. Guo, C. Zeng, C. Wang, L. Zhang, Investigation on efficient adsorption of cationic dyes on porous magnetic polyacrylamide microspheres, J. Hazard. Mater. 292 (2015) 90-97.
[4] D. Morshedi, Z. Mohammadi, M. M. A. Boojar, F. Aliakbari, Using protein nanofibrils to remove azo dyes from aqueous solution by the coagulation process, Colloids Surf. B. 112 (2013) 245-254.
[5] N. Al-Bastaki, Removal of methyl orange dye and Na_2SO_4 salt from synthetic waste water using reverse osmosis, Chem. Eng. Process, 43(12) (2004) 1561-1567.
[6] S. B. Hammouda, N. Adhoum, L. Monser, Chemical oxidation of a malodorous compound, indole, using iron entrapped in calcium alginate beads, J. Hazard. Mater. 301 (2016) 350-361.
[7] S. Wijannarong, S. Aroonsrimorakot, P. Thavipoke, S. Sangjan, Removal of reactive dyes from textile dyeing industrial effluent by ozonation process, APCBEE Procedia. 5 (2013) 279-282.
[8] C. Baslak, G. Arslan, M. Kus, Y. Cengeloglu, Removal of Rhodamine B from water by using CdTeSe quantum dot-cellulose membrane composites, RSC Adv. 6(22) (2016) 18549-18557.
[9] G. Darmograi, B. Prelot, A. Geneste, L.C. De Menorval, J. Zajac, Removal of three anionic orange-type dyes and Cr (VI) oxyanion from aqueous solutions onto strongly basic anion-exchange resin. The effect of single-component and competitive adsorption, Colloid Surf. A 508 (2016) 240-250.
[10] B.K. Körbahti, K. Artut, C. Geçgel, A. Özer, Electrochemical decolorization of textile dyes and removal of metal ions from textile dye and metal ion binary mixtures, chem. Eng. J. 173(3) (2011) 677-688.
[11] H. Mittal, S.S. Ray, A study on the adsorption of methylene blue onto gum ghatti/TiO2 nanoparticles-based hydrogel nanocomposite, Int. J. Biol. Macromol. 88 (2016) 66-80.
[12] N.V. Chagas, S.P. Quinaia, F.J. Anaissi, J.M. Santos, M.L. Felsner, K.C. Justi, Clay and charcoal composites: characterisation and application of factorial design analysis for dye adsorption, Chem. Pap. 68(4) (2014) 553-563.
[13] J. Fang, X. Huang, X. Ouyang, X. Wang, Study of the preparation of γ-Al_2O_3 nano-structured hierarchical hollow microspheres with a simple hydrothermal synthesis using methylene blue as structure directing agent and their adsorption enhancement for the dye, chem. Eng. J. 270 (2015) 309-319.
[14] Z. Ma, W. Chen, Z. Hu, X. Pan, G. Dong, S. Zhou, J. Qiu, Flexible and thermally stable SiO_2–TiO_2 composite micro fibers with hierarchical nano-heterostructure, RSC Adv. 3(43) (2013) 20132-20137.
[15] G. Allaedini, S.M. Tasirin, P. Aminayi, Synthesis of Fe–Ni–Ce trimetallic catalyst nanoparticles via impregnation and co-precipitation and their application to dye degradation, Chem. Pap. 70(2) (2016) 231-242.
[16] R. Ansari, Z. Mosayebzadeh, Application of polyaniline as an efficient and novel adsorbent for azo dyes removal from textile wastewaters, Chem. Pap. 65(1) (2011) 1-8.
[17] J. Tokarský, Čapková, Structure compatibility of TiO_2 and SiO_2 surfaces, Appl. Surf. Sci. 284 (2013) 55-164.
[18] L. Zhang, Y. Zhang, Adsorption characteristics of hexavalent chromium on HCB/TiO_2, Appl. Surf. Sci. 316 (2014) 649-656.
[19] F. Liu, Z. Guo, H. Ling, Z. Huang, D. Tang, Effect of pore structure on the adsorption of aqueous dyes to ordered mesoporous carbons, Microporous Mesoporous Mater. 227 (2016) 104-111.
[20] A. Šuligoj, U. Štangar, N. Tušar, Photocatalytic air-cleaning using TiO_2 nanoparticles in porous silica substrate, Chem. Pap. 68(9) (2014) 1265-1272.
[21] K.P.O. Mahesh, D.H. Kuo, B.R. Huang, Facile synthesis of hetero structured Ag-deposited SiO_2@TiO_2 composite spheres with enhanced catalytic activity towards the photodegradation of AB1 dye, J. Mol. Catal. A: Chem. 396 (2015) 290-296.
[22] X. Wang, M. Xi, X. Wang, H. Fong, Z. Zhu, Flexible composite felt of electrospun TiO_2 and SiO_2 nanofibers infused with TiO_2 nanoparticles for lithium ion battery anode, Electrochim. Acta. 190 (2016) 811-816.
[23] C. Ratiu, F. Manea, C. Lazau, C. Orha, G. Burtica, I. Grozescu, J. Schoonman, Photocatalytically-assisted electrochemical degradation of p-aminophenol in

aqueous solutions using zeolite-supported TiO_2 catalyst, Chem. Pap. 65(3) (2011) 289-298.
[24] M. Jabłońska, Selective catalytic oxidation of ammonia into nitrogen and water vapour over transition metals modified Al_2O_3, TiO_2 and ZrO_2, Chem. Pap. 69(9) (2015) 1141-1155.
[25] A. Amlouk, L. El Mir, S. Kraiem, S. Alaya, Elaboration and characterization of TiO2 nanoparticles incorporated in SiO_2 host matrix, J. Phys. Chem. Solids 67(7) (2006) 1464-1468.
[26] T. Suprabha, H.G. Roy, J. Thomas, K.P. Kumar, S. Mathew, Microwave-assisted synthesis of titania nanocubes, nanospheres and nanorods for photocatalytic dye degradation, Nanoscale Res. Lett. 4(2) (2009) 144-152.
[27] L. Zhang, Z. Xing, H. Zhang, Z. Li, X. Wu, X. Zhang, W. Zhou, High thermostable ordered mesoporous SiO_2–TiO_2 coated circulating-bed biofilm reactor for unpredictable photocatalytic and biocatalytic performance, Appl. Catal. B, 180 (2016) 521-529.
[28] A. Peter, L. Mihaly-Cozmuta, A. Mihaly-Cozmuta, C. Nicula, A. Jastrzębska, P. Kurtycz, A. Olszyna, Morphology, structure, and photoactivity of two types of graphene oxide–TiO_2 composites, Chem Pap. 69(6) (2015) 839-855.
[29] S. Ullah, E.P. Ferreira-Neto, A.A. Pasa, C.C. Alcântara, J.J. Acuna, S.A. Bilmes, U.P Rodrigues-Filho, Enhanced photocatalytic properties of core@ shell SiO_2@TiO_2 nanoparticles, Appl Catal. B. 179(2015) 333-343.
[30] J. Chen, J. Feng, W. Yan, Influence of metal oxides on the adsorption characteristics of PPy/metal oxides for Methylene Blue, J. Colloid Interf. Sci. 475 (2016) 26-35.
[31] K.P.O. Mahesh, D.H. Kuo, B.R. Huang, M. Ujihara, T. Imae, Chemically modified polyurethane-SiO_2/TiO_2 hybrid composite film and its reusability for photocatalytic degradation of Acid Black 1 (AB1) under UV light, Appl. Catal. A, 475 (2014) 235-241.
[32] H. Wang, H. Gao, M. Chen, X. Xu, X. Wang, C. Pan, J. Gao, Microwave-assisted synthesis of reduced graphene oxide/titania nanocomposites as an adsorbent for methylene blue adsorption, Appl. Surf. Sci. 360 (2016) 840-848.
[33] L. Li, S. Zhou, E. Chen, R. Qiao, Y. Zhong, Y. Zhang, Z. Li, Simultaneous formation of silica-protected and N-doped TiO_2 hollow spheres using organic–inorganic silica as self-removed templates, J. Mater. Chem. A 3(5) (2015) 2234-2241.
[34] A.C.M. Oliveira, M.S. Santos, L.M. Brandão, R.N. Yerga, J.L.G. Fierro, M.S. Leite, R.T. Figueiredo, Chitosan-modified TiO_2 as photocatalyst for ethanol reforming under visible light, Chem. Pap. 71(6) (2017) 1129-1141.
[35] X.H. Yang, H.T. Fu, X.Z. An, X.C. Jiang, A.B. Yu, Synthesis of V_2O_5@TiO_2 core–shell hybrid composites for sunlight degradation of methylene blue, RSC Adv. 6(41) (2016) 34103-34109.
[36] K.V. Bineesh, D.K. Kim, D.W. Park, Synthesis and characterization of zirconium-doped mesoporous nano-crystalline TiO_2, Nanoscale 2(7) (2010) 1222-1228.
[37] M. Pal, U. Pal, J.M.G.Y. Jiménez, F. Pérez-Rodríguez, Effects of crystallization and dopant concentration on the emission behavior of TiO_2: Eu nanophosphors, Nanoscale Res. Lett. 7(1) (2012) 1-12.
[38] O.A. Zelekew, D.H. Kuo, A two-oxide nanodiode system made of double-layered p-type Ag_2O@n-type TiO_2 for rapid reduction of 4-nitrophenol, Phys. Chem. Chem. Phys. 18(6) (2016) 4405-4414.
[39] H.S. Kibombo, R. Peng, S. Rasalingam, R.T. Koodali, Versatility of heterogeneous photocatalysis: synthetic methodologies epitomizing the role of silica support in TiO_2 based mixed oxides, Catal. Sci. Technol. 2(9) (2012) 1737-1766.
[40] S.S.P. Selvin, N. Radhika, O. Borang, I.S. Lydia, J.P. Merlin, Visible light driven photodegradation of Rhodamine B using cysteine capped ZnO/GO nanocomposite as photocatalyst, J. Mater. Sci. Mater. Electron. 28(9) (2017) 6722-6730.
[41] P.V. Messina, P.C. Schulz, Adsorption of reactive dyes on titania–silica mesoporous materials, J. Colloid Interf. Sci. 299(1) (2006) 305-320.
[42] A. Mittal, J. Mittal, A. Malviya, D. Kaur, V.K. Gupta, Adsorption of hazardous dye crystal violet from wastewater by waste materials, J. Colloid Interf. Sci. 343(2) (2010) 463-473.
[43] Y. Yao, F. Xu, M. Chen, Z. Xu, Z. Zhu, Adsorption behavior of methylene blue on carbon nanotubes, Bioresour. Technol. 101(9) (2010) 3040-3046.
[44] T.S. Natarajan, H.C. Bajaj, R.J. Tayade, Preferential adsorption behavior of methylene blue dye onto surface hydroxyl group enriched TiO_2 nanotube and its photocatalytic regeneration, J. Colloid Interf. Sci. 433(2014) 104-114.
[45] R. Pandimurugan, S. Thambidurai, Synthesis of seaweed-ZnO-PANI hybrid composite for adsorption of methylene blue dye, J. Environ. Chem. Eng. 4(1) (2016) 1332-1347.
[46] H. Aysan, S. Edebali, C. Ozdemir, M.C. Karakaya, N. Karakaya, Use of chabazite, a naturally abundant zeolite, for the investigation of the adsorption kinetics and mechanism of methylene blue dye, Microporous Mesoporous Mater. 235 (2016) 78-86.
[47] J. Qin, F. Qiu, X. Rong, J. Yan, H. Zhao, D. Yang, Adsorption behavior of crystal violet from aqueous solutions with chitosan–graphite oxide modified polyurethane as an adsorbent, J. Appl. Polym. Sci. 132(17) (2015) 41828-41837.
[48] K.P. Singh, S. Gupta, A.K. Singh, S. Sinha, Optimizing adsorption of crystal violet dye from water by magnetic nanocomposite using response surface modeling approach, J. Hazard. Mater. 186(2) (2011) 1462-1473.
[49] T.S. Anirudhan, M. Ramachandran, Adsorptive removal of basic dyes from aqueous solutions by surfactant modified bentonite clay (organoclay): kinetic and competitive adsorption isotherm, Proc. Saf. Environ. Prot. 95 (2015) 215-225.
[50] V. Sabna, S.G. Thampi, S. Chandrakaran, Adsorption of crystal violet onto functionalised multi-walled carbon nanotubes: Equilibrium and kinetic studies, Ecotoxicol. Environ. Saf. 134 (2016) 390-397.
[51] C. Muthukumaran, V.M. Sivakumar, M. Thirumarimurugan, Adsorption isotherms and kinetic studies of crystal violet dye removal from aqueous solution using surfactant modified magnetic nanoadsorbent, J. Taiwan Inst. Chem. Eng. 63 (2016) 354-362.
[52] R.F. Mansa, C.S. Sipaut, I.A. Rahman, N.S.M. Yusof, M. Jafarzadeh, Preparation of glycine–modified silica nanoparticles for the adsorption of malachite green dye, J. Porous Mater. 23(1) (2016) 35-46.
[53] G.K. Sarma, S.S. Gupta, K.G. Bhattacharyya, Adsorption of crystal violet on raw and acid-treated montmorillonite, K10, in aqueous suspension, J. Environ. Manage. 171 (2016) 1-10.
[54] H.K. Boparai, M. Joseph, D.M. O'Carroll, Kinetics and thermodynamics of cadmium ion removal by adsorption onto nano zerovalent iron particles, J. Hazard. Mater. 186(1) (2011) 458-465.
[55] V.O. Njoku, K.Y. Foo, M. Asif, B.H. Hameed, Preparation of activated carbons from rambutan (Nephelium lappaceum) peel by microwave-induced KOH activation for acid yellow 17 dye adsorption, Chem. Eng. J. 250 (2014) 198-204.
[56] M. Ghaedi, A.M. Ghaedi, M. Hossainpour, A. Ansari, M.H. Habibi, A.R. Asghari, Least square-support vector (LS-SVM) method for modeling of methylene blue dye adsorption using copper oxide loaded on activated carbon: Kinetic and isotherm study, Ind. Eng. Chem. Res. 20(4) (2014) 1641-1649.
[57] H. Chaudhuri, S. Dash, A. Sarkar, Adsorption of different dyes from aqueous solution using Si-MCM-41 having very high surface area, J. Porous Mater. 23(5) (2016) 1227-1237
[58] R. Hazzaa, M. Hussein, Adsorption of cationic dye from aqueous solution onto activated carbon prepared from olive stones, Environ. Technol. Innovat. 4 (2015) 36-51.
[59] E.A.N. Simonetti, L. de Simone Cividanes, T.M.B. Campos, B.R.C. de Menezes, F.S. Brito, G.P. Thim, Carbon and TiO_2 synergistic effect on methylene blue adsorption, Mater. Chem. Phys. 177 (2016) 330-338.
[60] M. Iram, C. Guo, Y. Guan, A. Ishfaq, H. Liu, Adsorption and magnetic removal of neutral red dye from aqueous solution using Fe_3O_4 hollow nanospheres, J. Hazard. Mater. 181(1) (2010) 1039-1050.
[61] M. Jose, M. Kumari, R. Karunakaran, S. Shukla, Methylene blue adsorption from aqueous solutions using undoped and silver-doped nanotubes of anatase-titania synthesized via modified hydrothermal method, J. Sol-Gel Sci. Technol. 75(3) (2015) 541-550.
[62] M.G. Vaz, A.G. Pereira, A.R. Fajardo, A.C. Azevedo, F.H. Rodrigues, Methylene blue adsorption on chitosan-g-poly (acrylic acid)/rice husk ash superabsorbent composite: kinetics, equilibrium, and thermodynamics, Water Air Soil Pollut. 228(1) (2017) 1-13.
[63] M. Auta, B.H. Hameed, Modified mesoporous clay adsorbent for adsorption isotherm and kinetics of methylene blue, Chem. Eng. J. 198 (2012) 219-227.
[64] H. Zhao, F. Qiu, J. Yan, J. Wang, X. Li, D. Yang, Preparation of economical and environmentally friendly graphene/palygorskite/TiO_2 composites and its application for the removal of methylene blue, Appl. Clay Sci. 121 (2016) 137-145.
[65] J. Feng, J. Zhu, W. Lv, J. Li, W. Yan, Effect of hydroxyl group of carboxylic acids on the adsorption of acid red G and methylene blue on TiO_2, Chem. Eng. J. 269 (2015) 316-322.